

Palladium Anchored Donor Flexible Pyridylidene Amide (PYA) Electrocatalysts for CO₂ Reduction

Afshan Khurshid^{†a}, Tania Tanveer^{†a}, Komal Hafeez^{†a}, Maqsood Ahmed^b, Zareen Akhtar^a, M.

Naveed Zafar^{a*}

^a Department of Chemistry, Quaid-i-Azam University, Islamabad, 45320, Pakistan

^b Materials Chemistry Laboratory, Department of Chemistry, The Islamia University of
Bahawalpur, 63100, Pakistan

[†]Authors contributed equally to this manuscript

*For correspondence, email to mnzafar@qau.edu.pk

Content	Pages
Figure S1.1. ¹ H NMR spectrum of 1	S3
Figure S1.2. ¹³ C NMR spectrum of 1	S3
Figure 1.3. Representative FT-IR spectrum of 1	S4
Figure S2.1. ¹ H NMR spectrum of 2	S4
Figure S2.2. ¹³ C NMR spectrum of 2	S5
Figure 2.3. Representative FT-IR spectrum of 2	S5
Figure S3.1. ¹ H NMR spectrum of 3	S6
Figure S3.2. ¹³ C NMR spectrum of 3	S6
Figure 3.3. Representative FT-IR spectrum of 3	S7
Figure S4.1. ¹ H NMR spectrum of 4	S7
Figure S4.2. ¹³ C NMR spectrum of 4	S8
Figure 4.3. Representative FT-IR spectrum of 4	S8
Figure S5.1. ¹ H NMR spectrum of 5	S9
Figure S5.2. ¹³ C NMR spectrum of 5	S9
Figure 5.3. Representative FT-IR spectrum of 5	S10
Figure S6.1. ¹ H NMR spectrum of 6	S10
Figure S6.2. ¹³ C NMR spectrum of 6	S11
Figure 6.3. Representative FT-IR spectrum of 6	S11
Figure S7.1. ¹ H NMR spectrum of 7	S12
Figure S7.2. ¹³ C NMR spectrum of 7	S12
Figure 7.3. Representative FT-IR spectrum of 7	S13
Figure S8.1. ¹ H NMR spectrum of 8	S13
Figure S8.2. ¹³ C NMR spectrum of 8	S14
Figure 8.3. Representative FT-IR spectrum of 8	S14
Figure S9.1. ¹ H NMR spectrum of 9	S15
Figure S9.2. ¹³ C NMR spectrum of 9	S15
Figure 9.3. Representative FT-IR spectrum of 9	S16

Figure S10.1. ^1H NMR spectrum of 10	S16
Figure S10.2. ^{13}C NMR spectrum of 10	S17
Figure 10.3. Representative FT-IR spectrum of 10	S17
Figure S11.1. ^1H NMR spectrum of 11	S18
Figure S11.2. ^{13}C NMR spectrum of 11	S18
Figure 11.3. Representative FT-IR spectrum of 11	S19
Crystals Data	S20
Figure S12. ORTEP diagrams of 2 and 4	S20
Figure S13. ORTEP diagrams of 11	S21
Electrochemical Data	S22
Figure S14. Cyclic voltammograms of 7 under nitrogen, CO_2 at different scan rates. All experiments were performed at 100 mVs^{-1} scan rate in DMF and 0.1 M supporting electrolyte $[\text{n Bu}_4\text{N}]\text{PF}_6$.	S22
Figure S15. Current <i>vs</i> (scan rate) $^{1/2}$ plots of 7 under nitrogen, CO_2 . All experiments were performed at 100 mVs^{-1} scan rate in DMF and 0.1 M supporting electrolyte $[\text{n Bu}_4\text{N}]\text{PF}_6$.	S23
Figure S16. Cyclic voltammograms of 9 under $\text{CO}_2 + \text{TFA}$ at different acid concentration. All experiments were performed at 100 mVs^{-1} scan rate in DMF and 0.1 M supporting electrolyte $[\text{n Bu}_4\text{N}]\text{PF}_6$	S23
References	S23

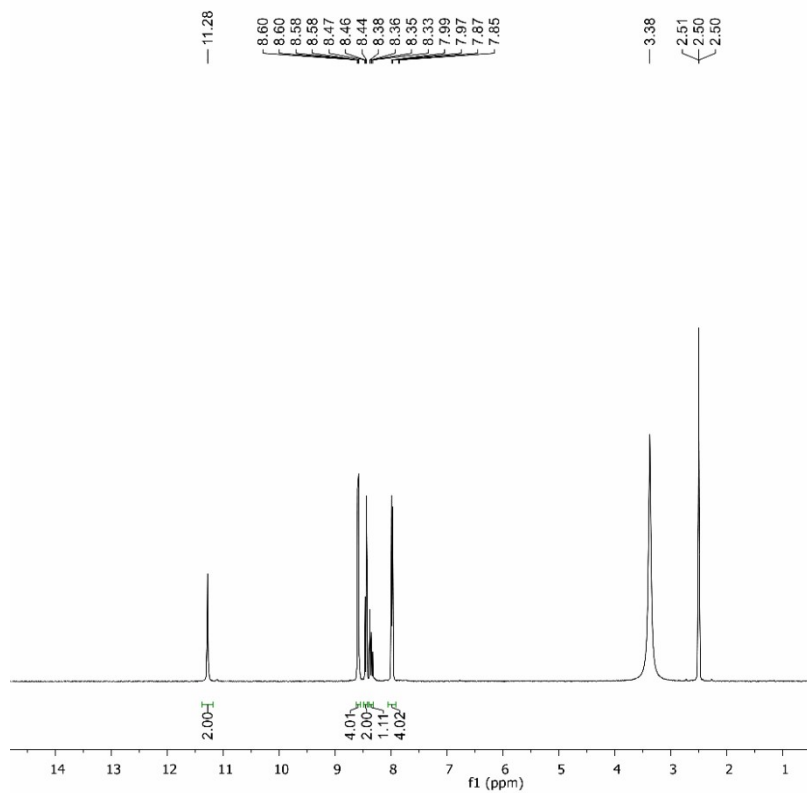


Figure 1.1 ^1H NMR spectrum of **1**

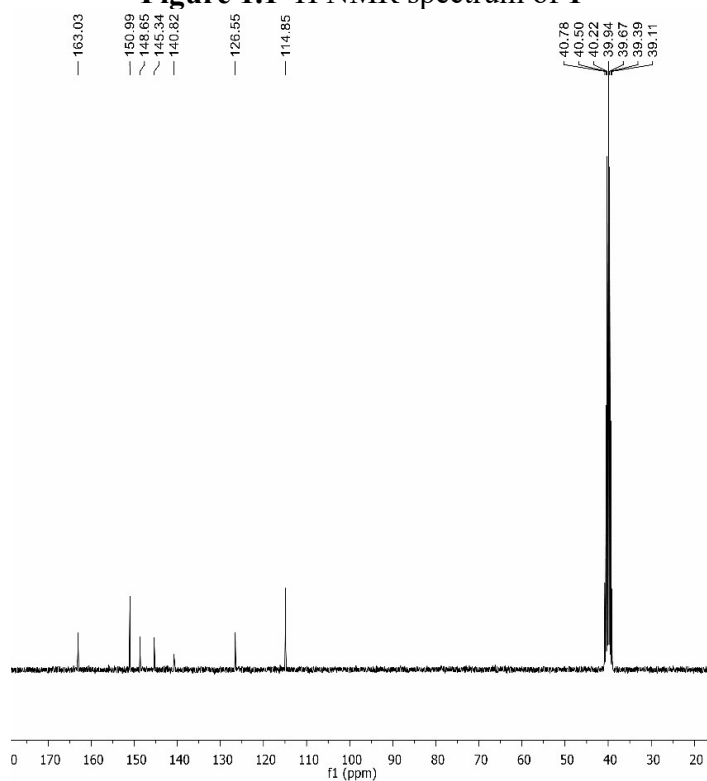


Figure 1.2 ^{13}C NMR spectrum of **1**

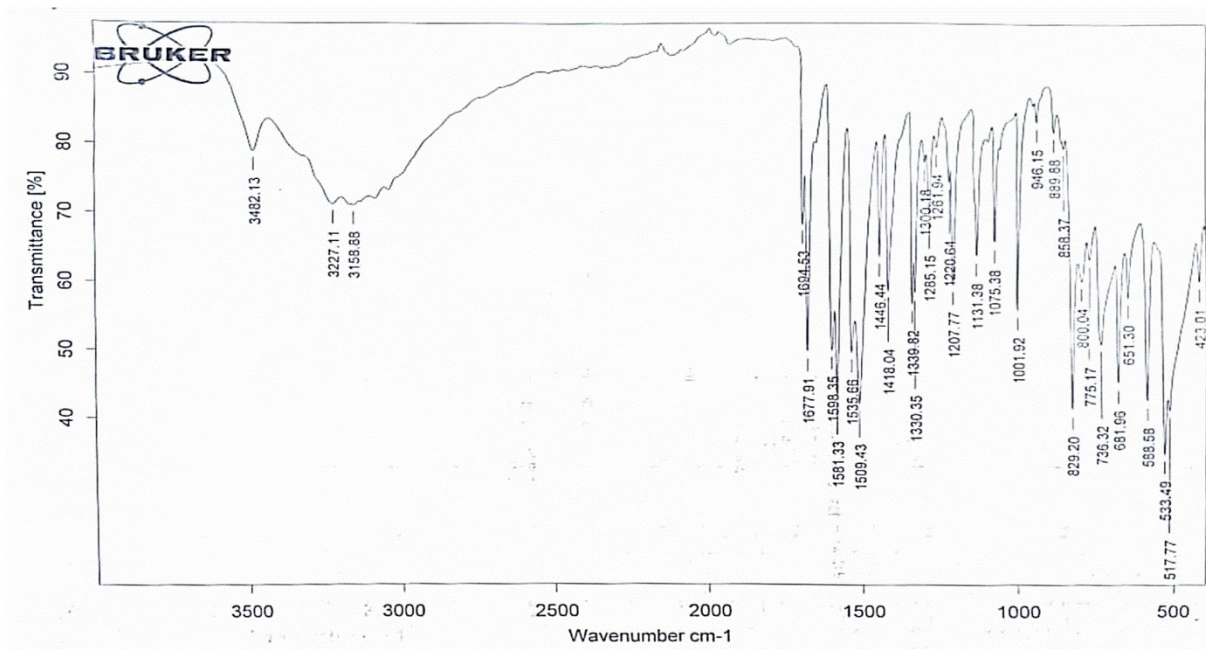


Figure 1.3. Representative FT-IR spectrum of 1

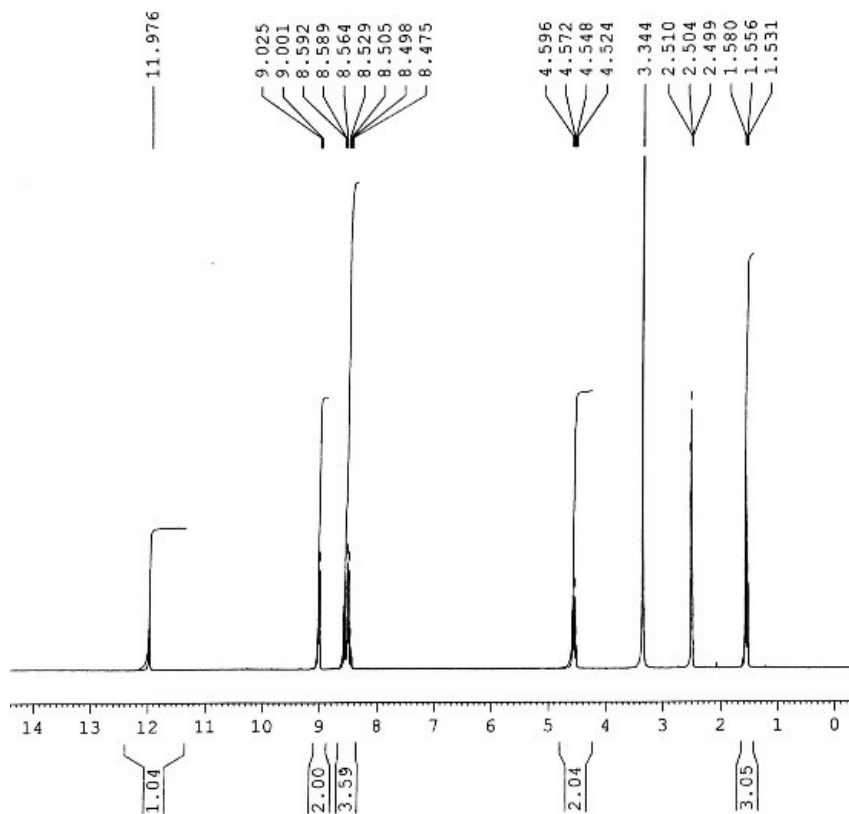


Figure 2.1 ¹H NMR spectrum of 2

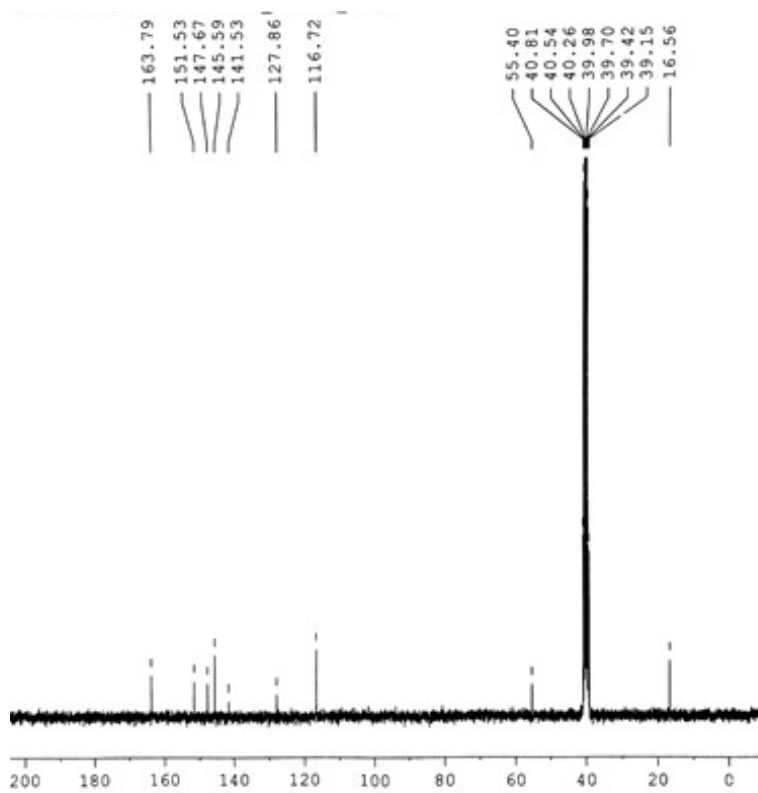


Figure 2.2 ^{13}C NMR spectrum of **2**

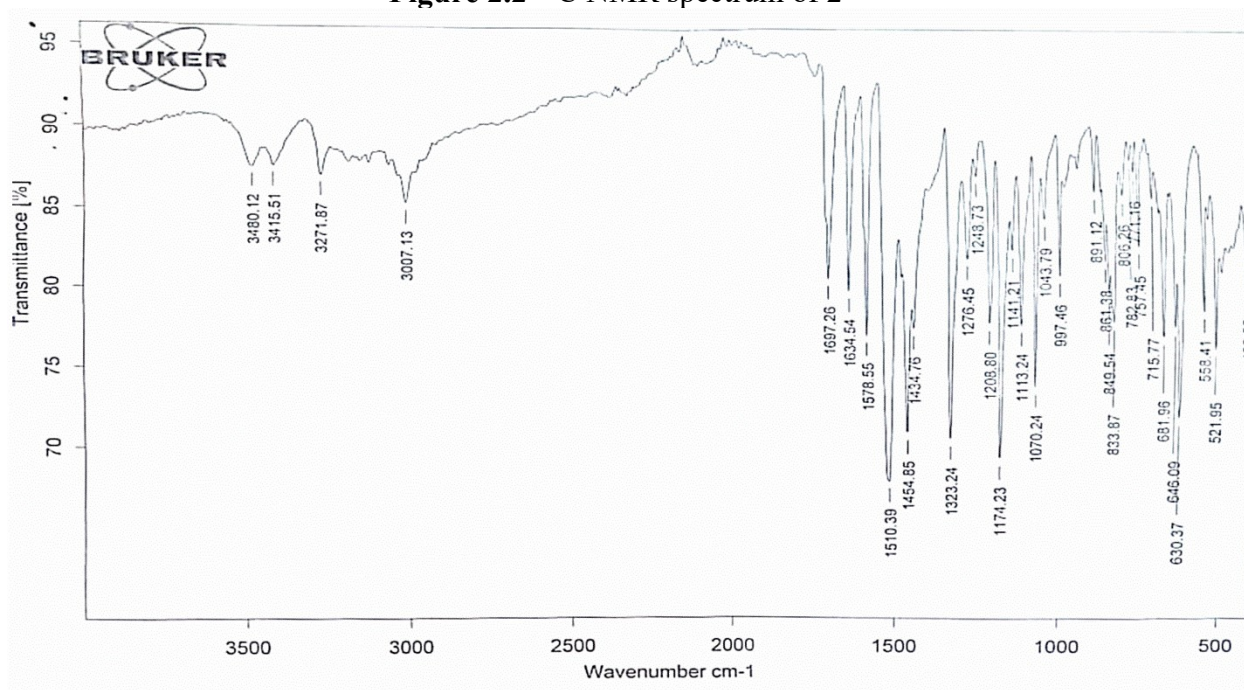


Figure 2.3. Representative FT-IR spectrum of **2**

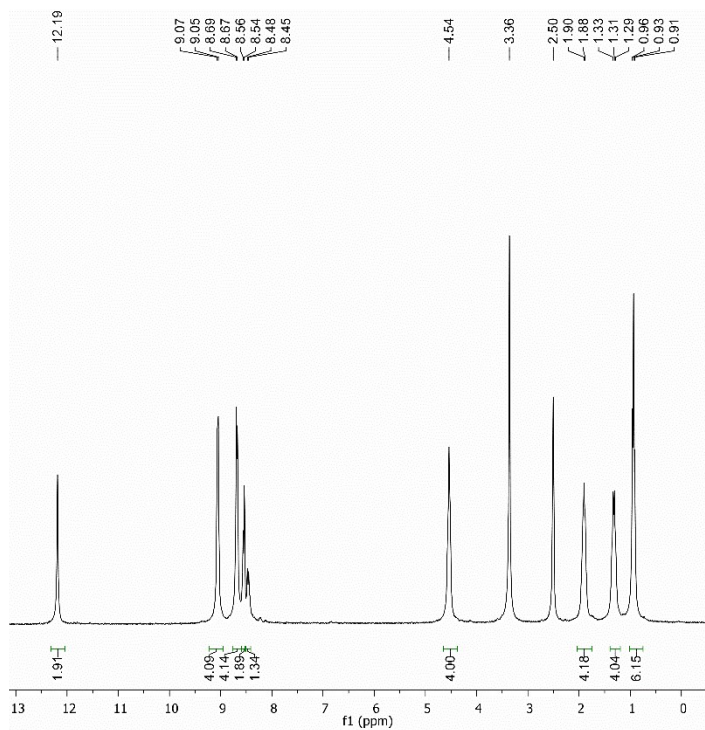


Figure 3.1. ^1H NMR spectrum of **3**

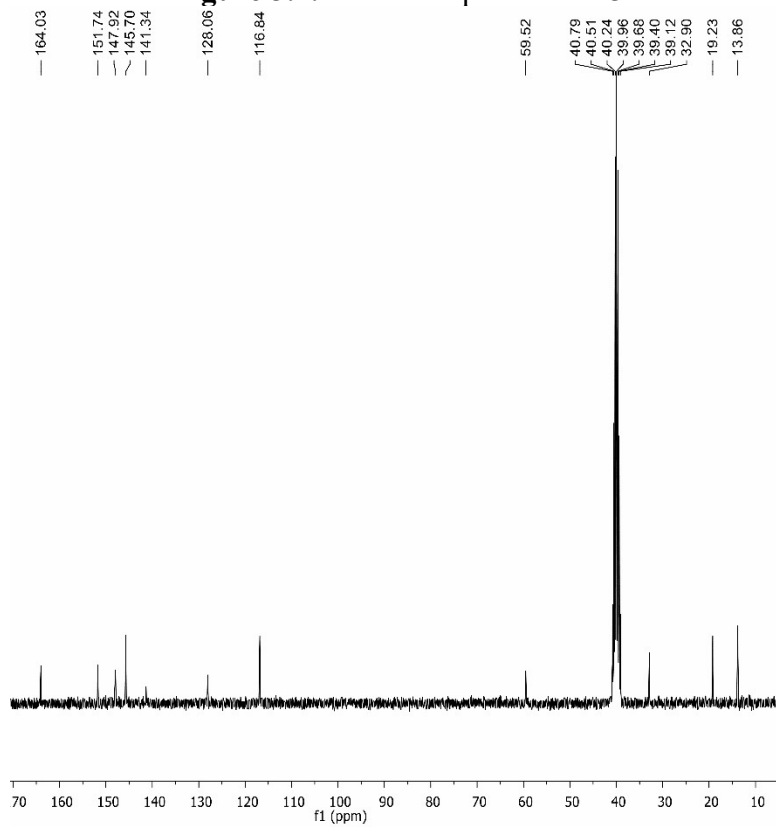


Figure 3.2. ^{13}C NMR spectrum of **3**

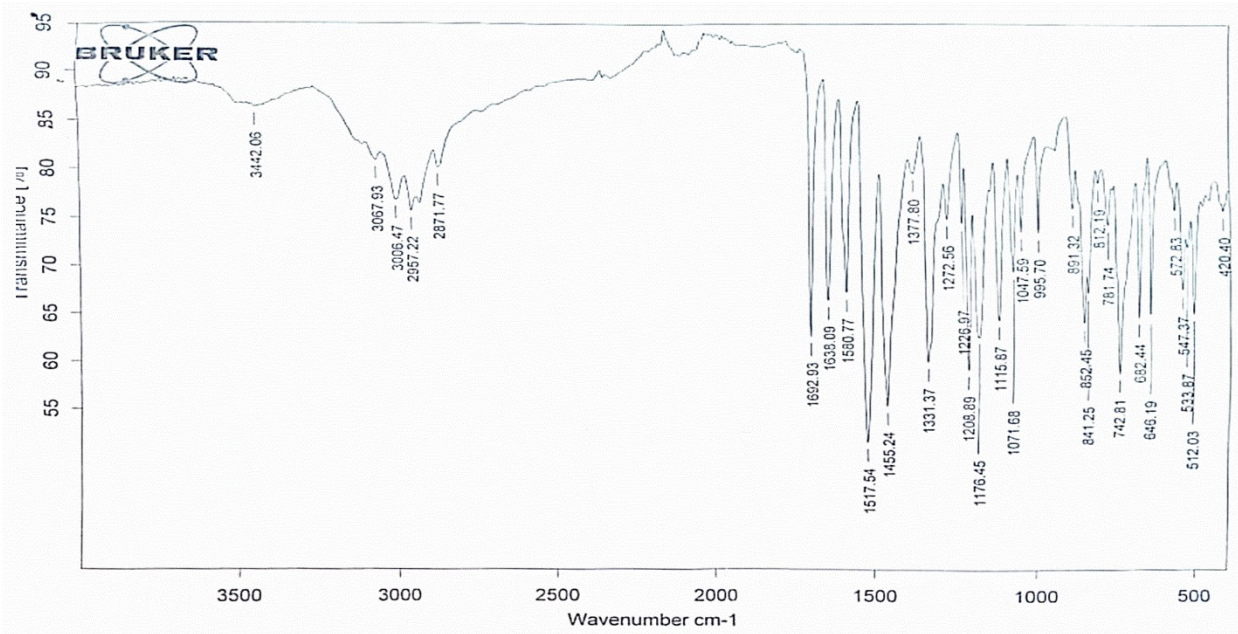


Figure 3.3. Representative FT-IR spectrum of **3**

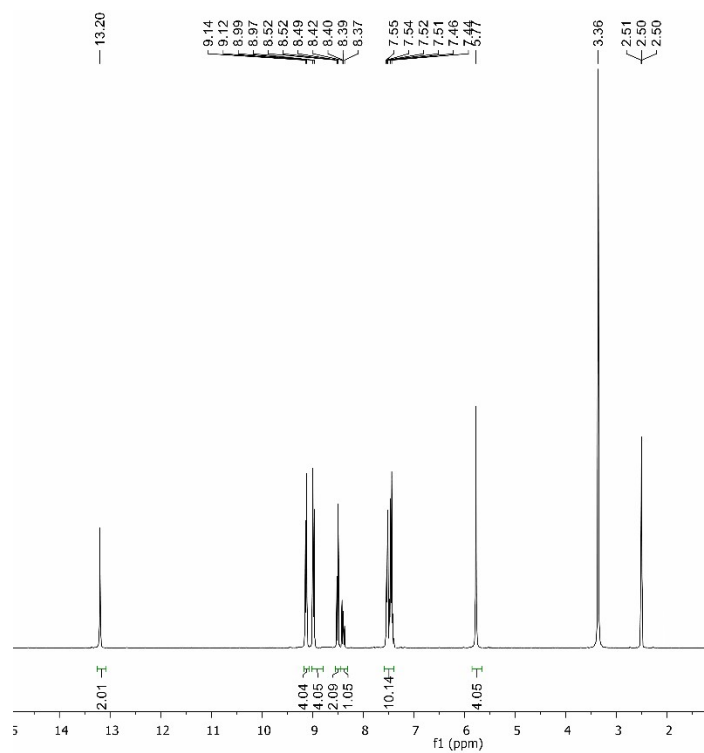


Figure 4.1. ^1H NMR spectrum of **4**

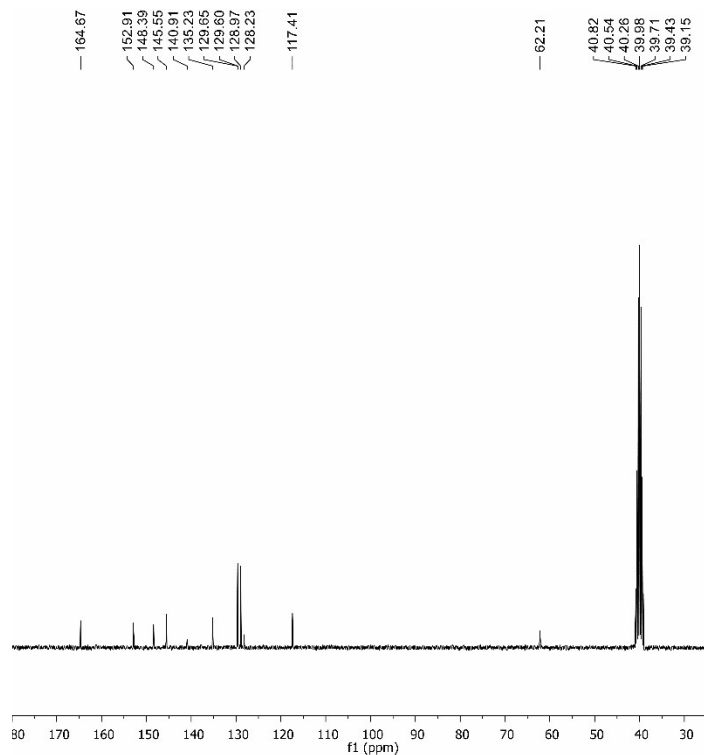


Figure 4.2. ^{13}C NMR spectrum of **4**

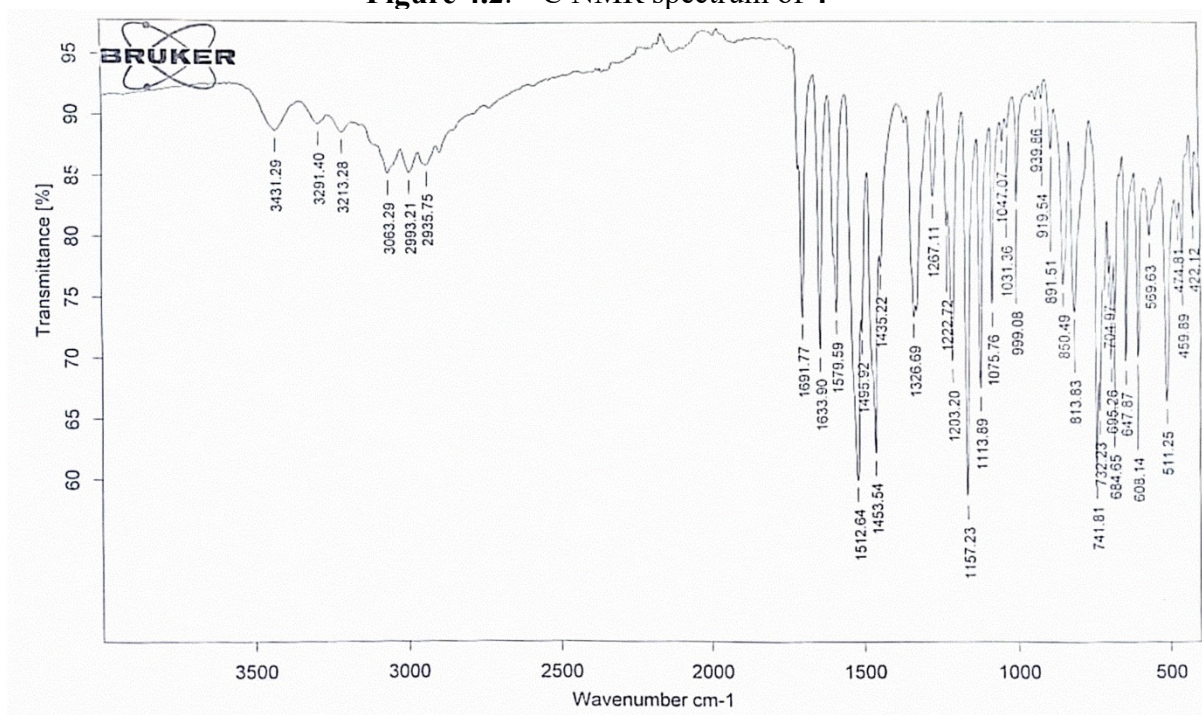


Figure 4.3. Representative FT-IR spectrum of **4**

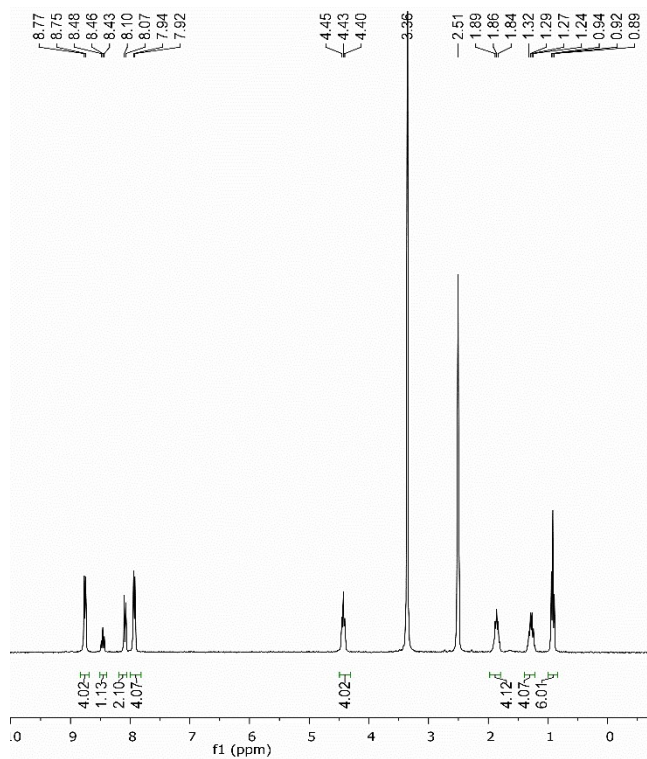


Figure 5.1. ^1H NMR spectrum of **5**

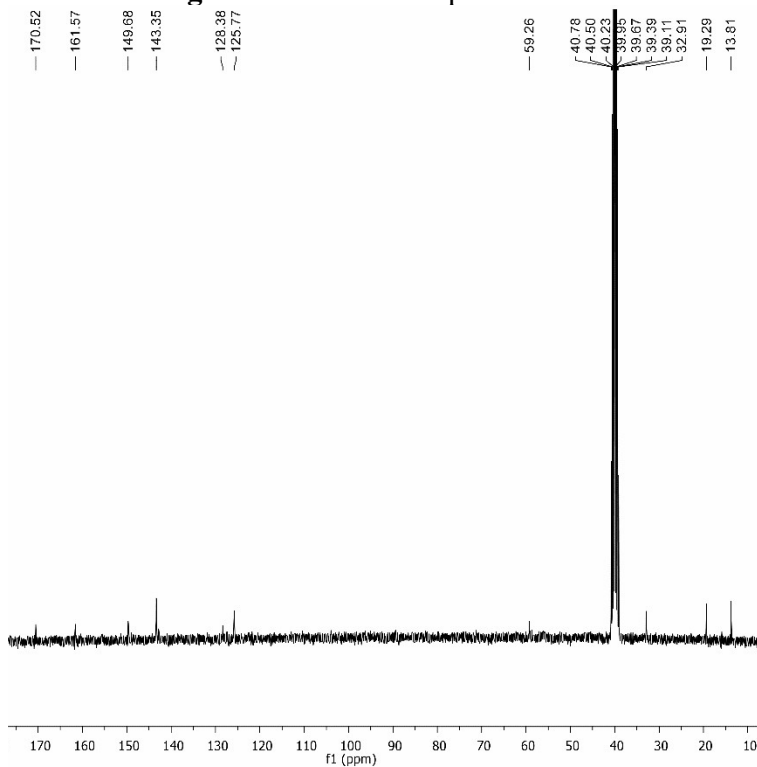


Figure 5.2. ^{13}C NMR spectrum of **5**

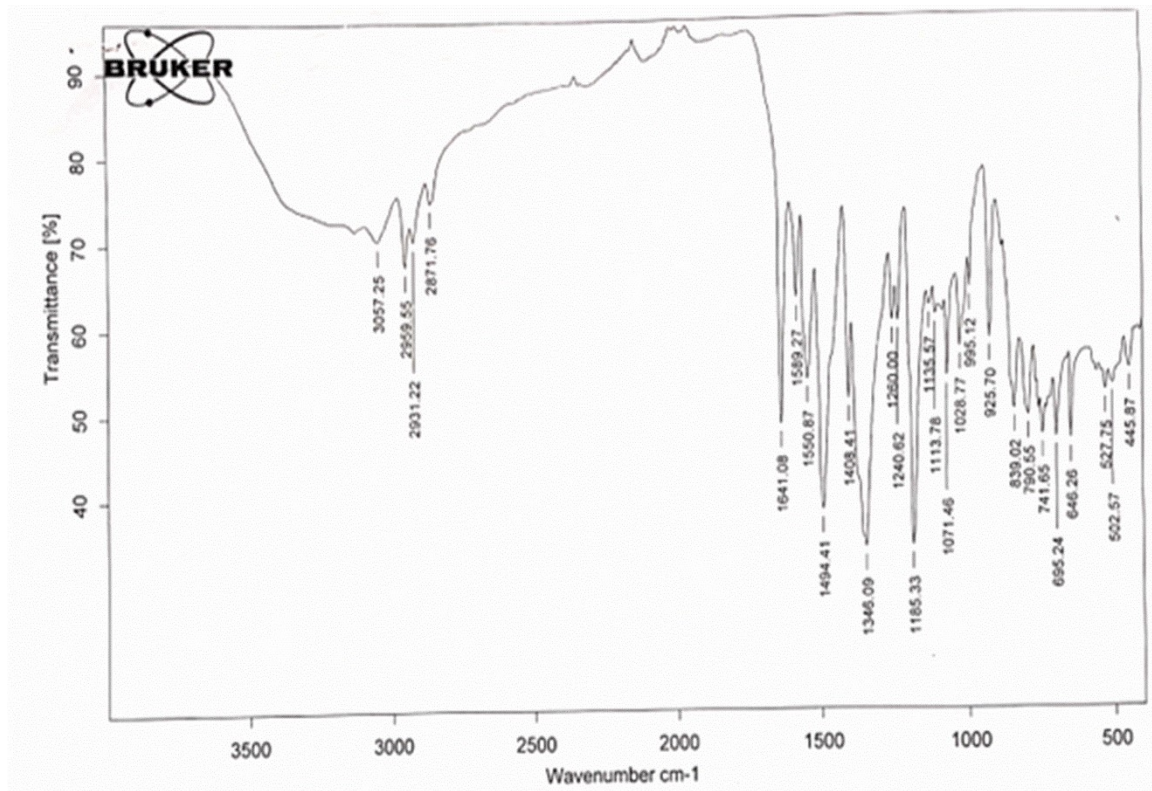


Figure 5.3. Representative FT-IR spectrum of 5

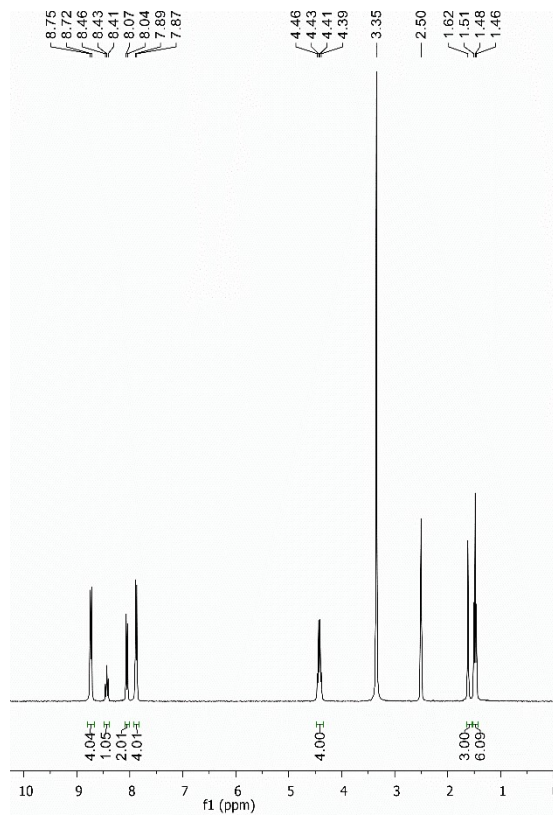


Figure 6.1. ¹H NMR spectrum of 6

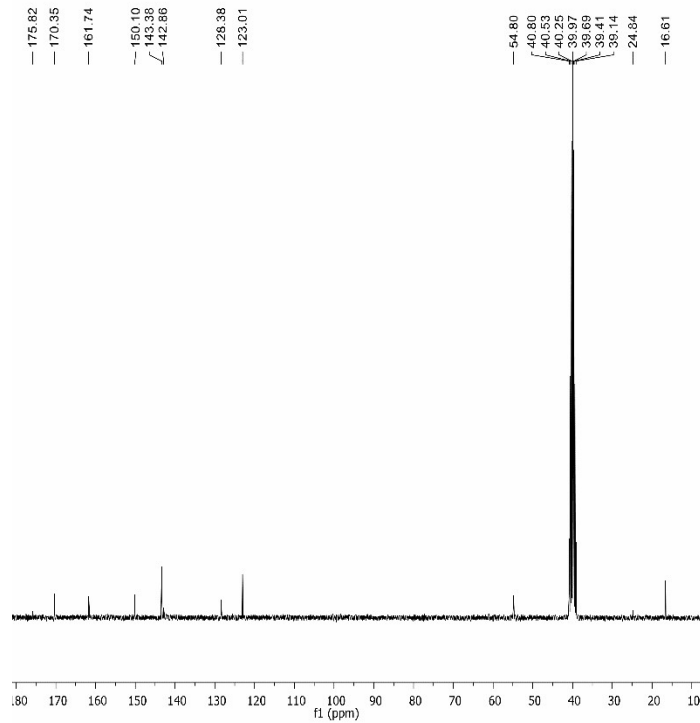


Figure 6.2. ¹³C NMR spectrum of 6

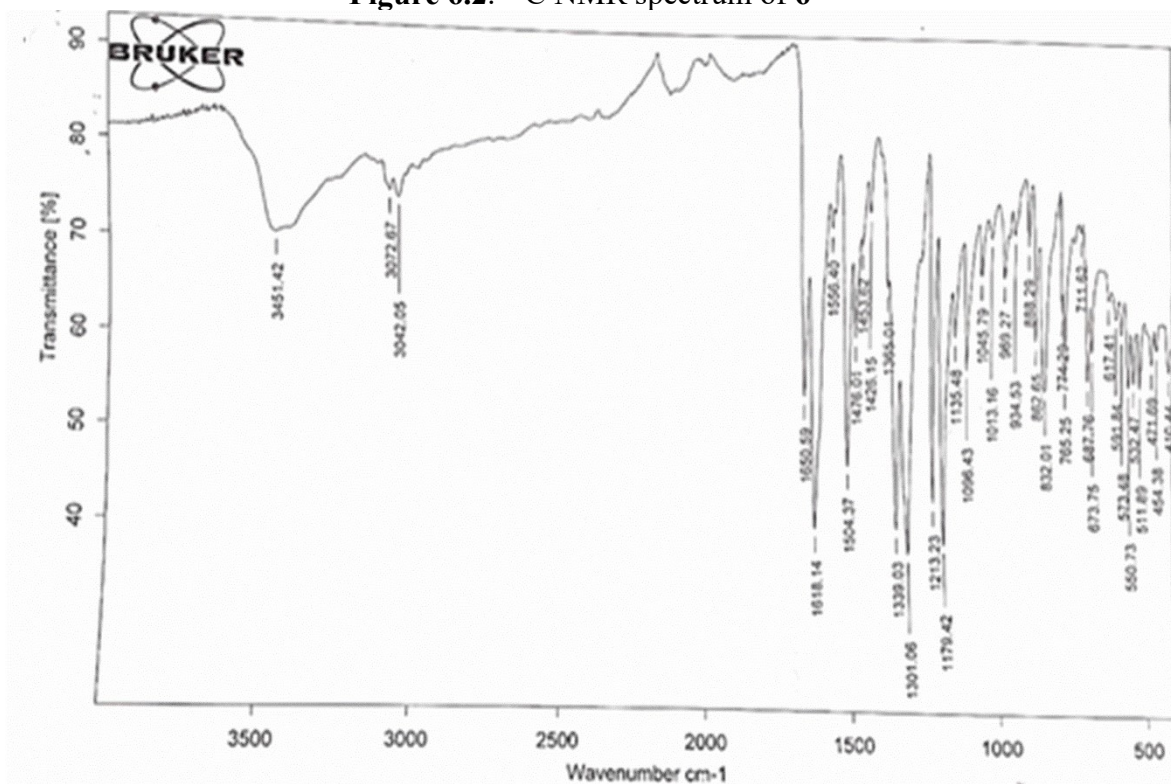


Figure 6.3. Representative FT-IR spectrum of 6

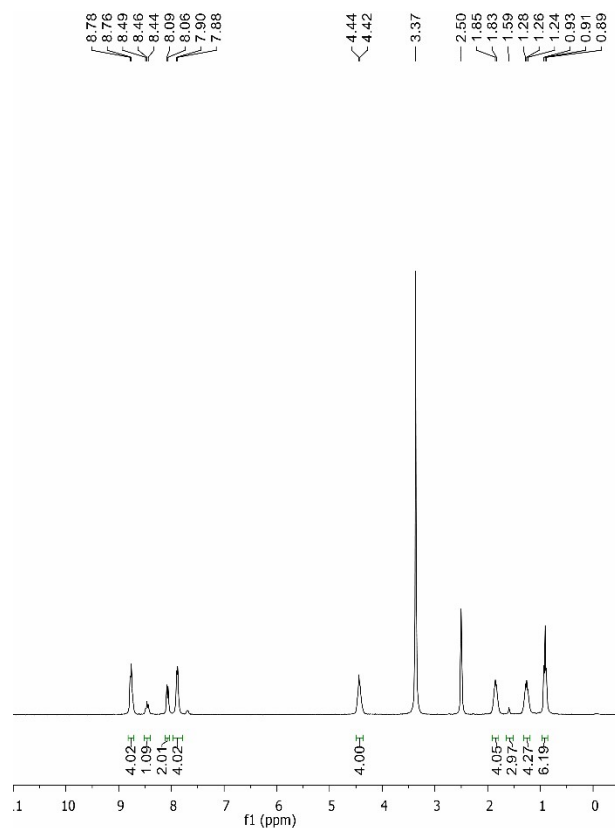


Figure 7.1. ^1H NMR spectrum of 7

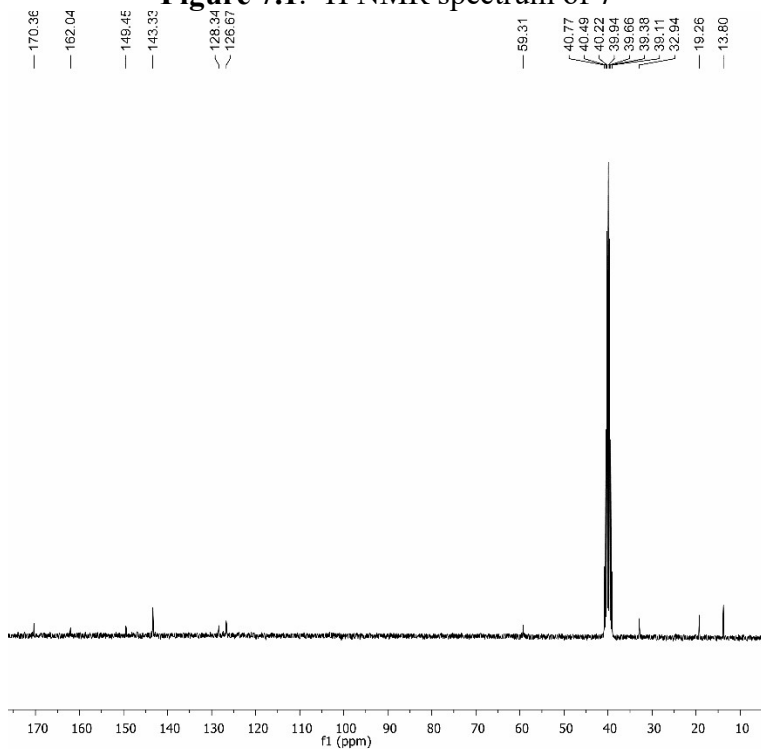


Figure 7.2. ^{13}C NMR spectrum of 7

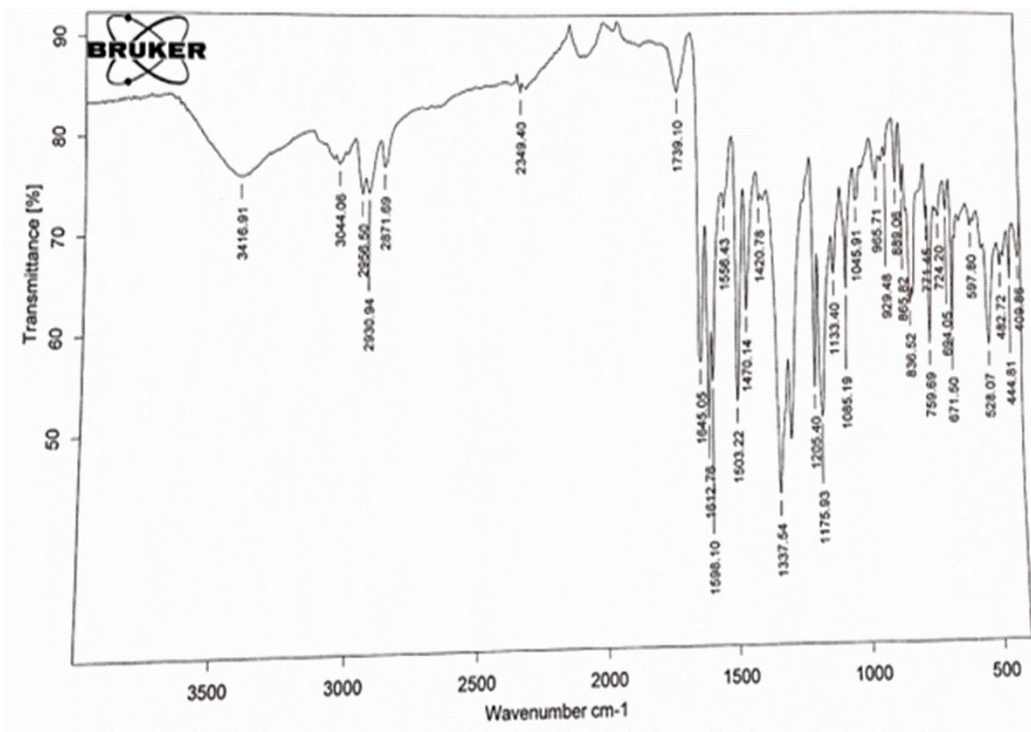


Figure 7.3. Representative FT-IR spectrum of 7

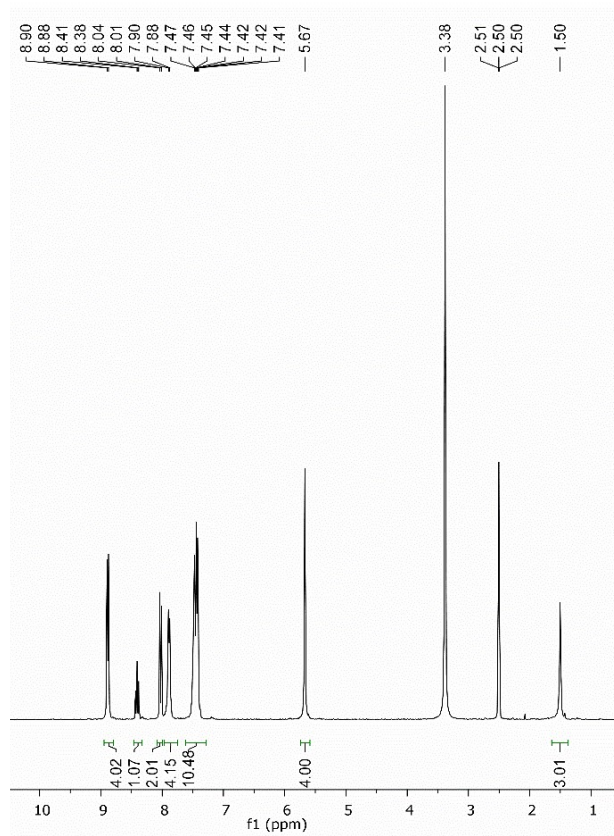


Figure 8.1. ¹H NMR spectrum of 8

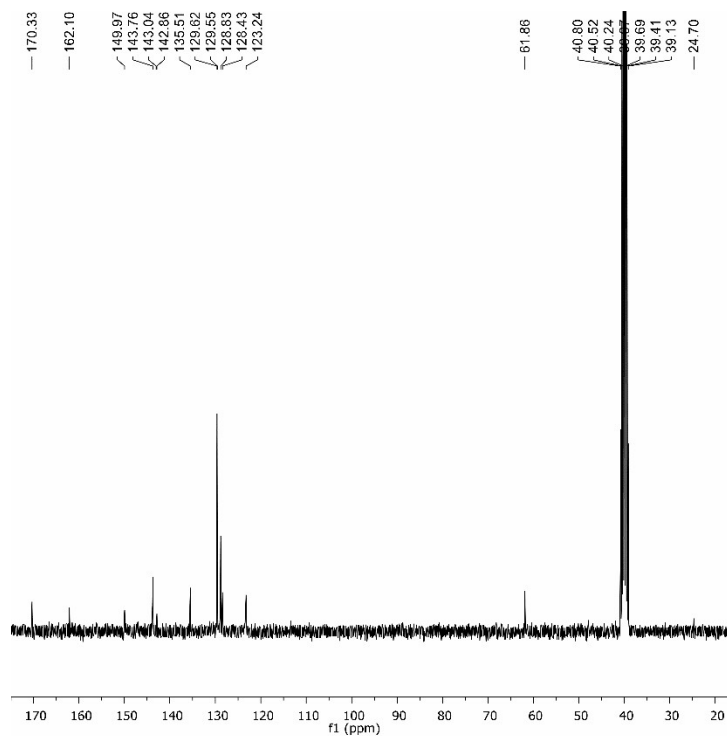


Figure 8.2. ^{13}C NMR spectrum of **8**

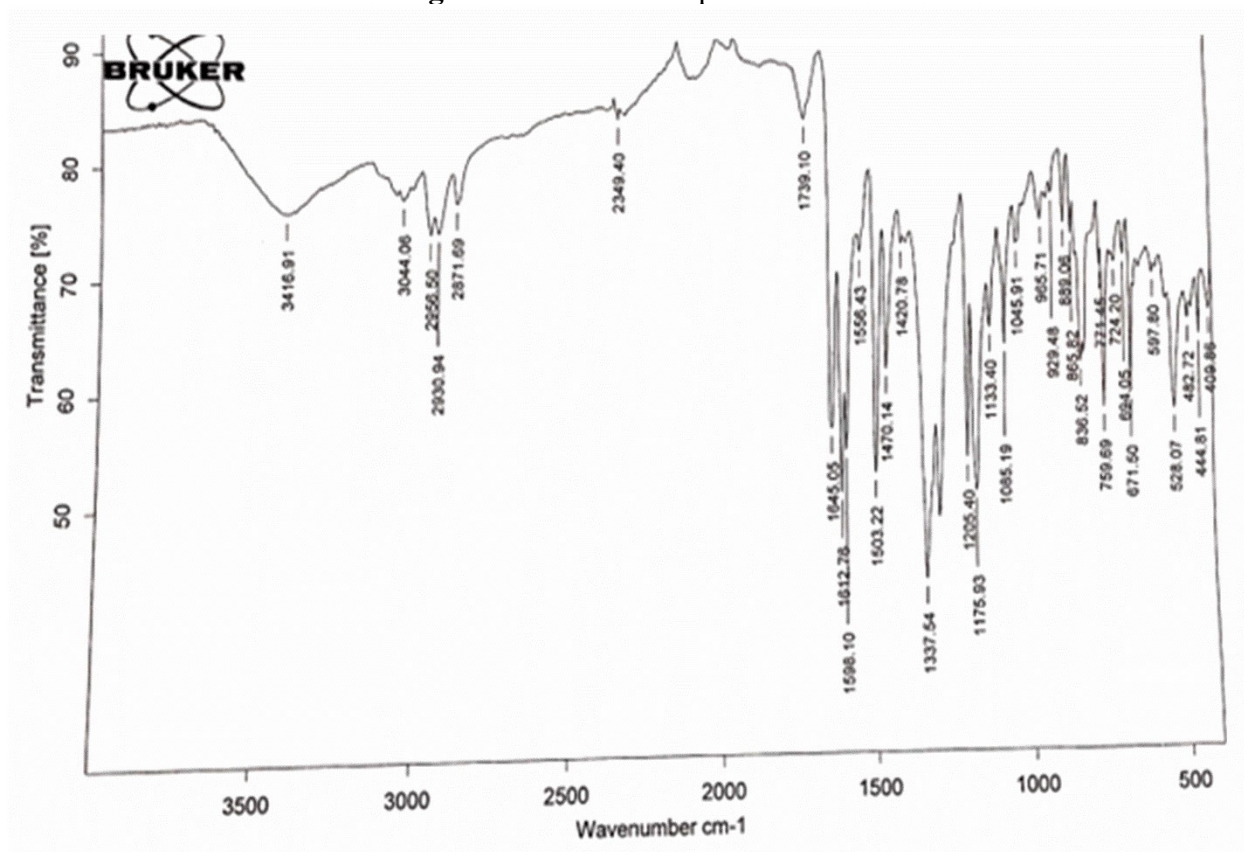


Figure 8.3. Representative FT-IR spectrum of **8**

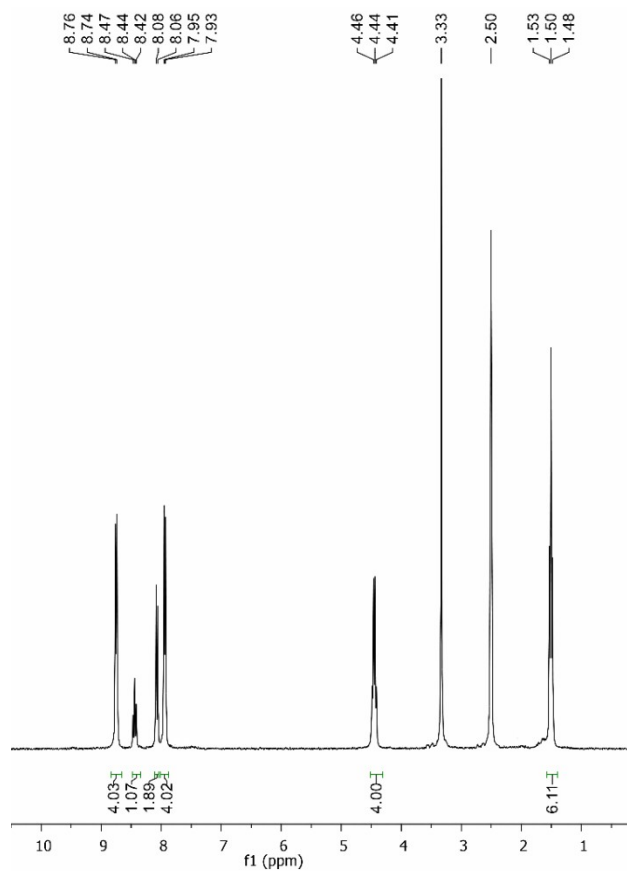


Figure 9.1. ^1H NMR spectrum of **9**

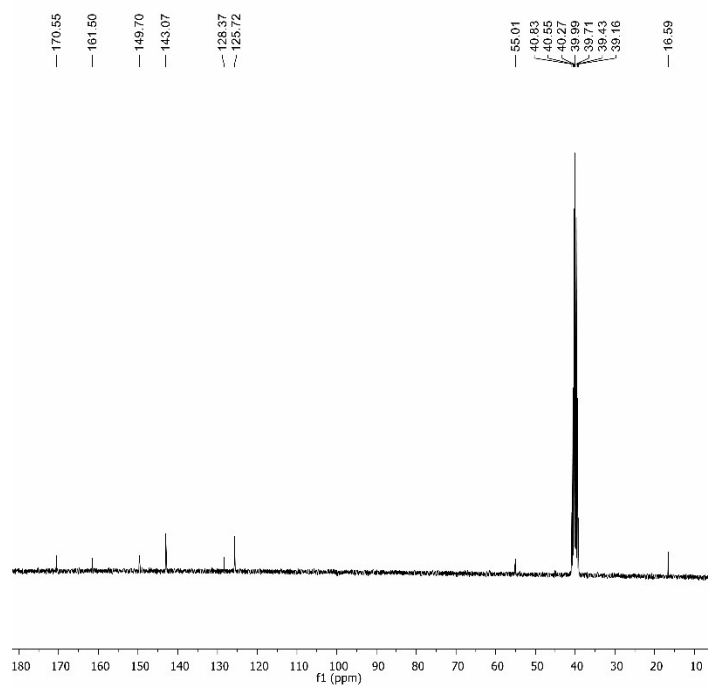


Figure 9.2. ^{13}C NMR spectrum of **9**

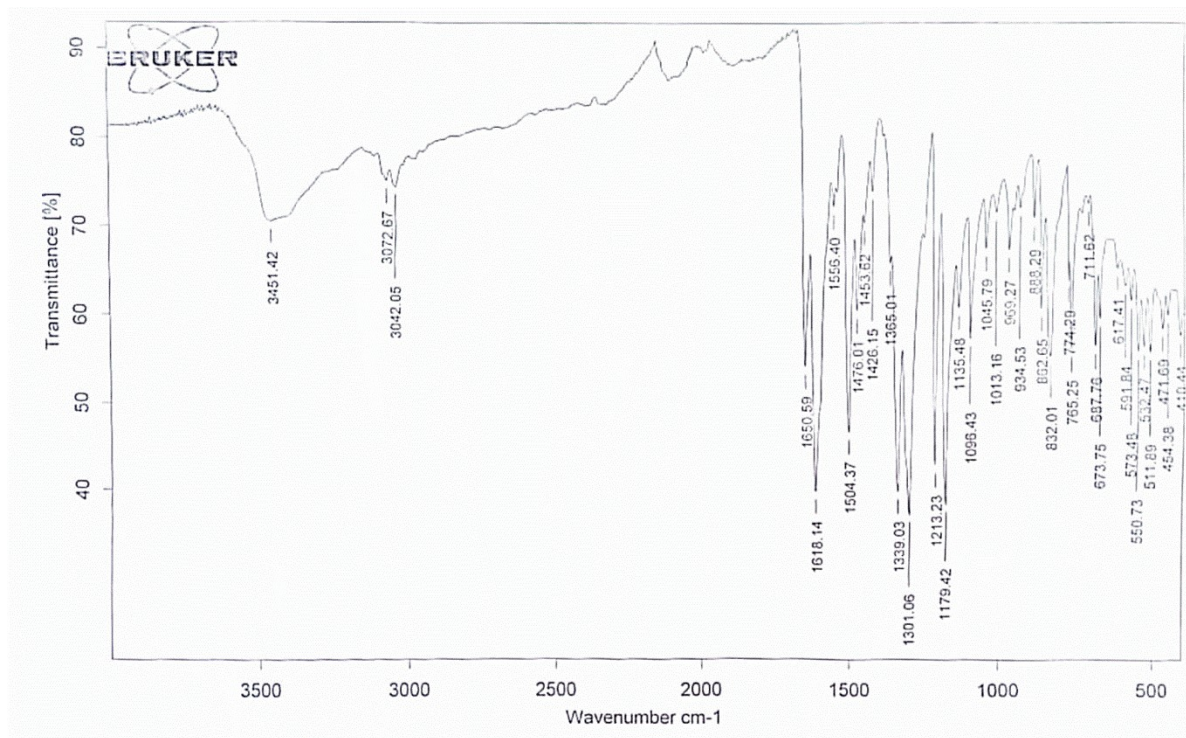


Figure 9.3. Representative FT-IR spectrum of **9**

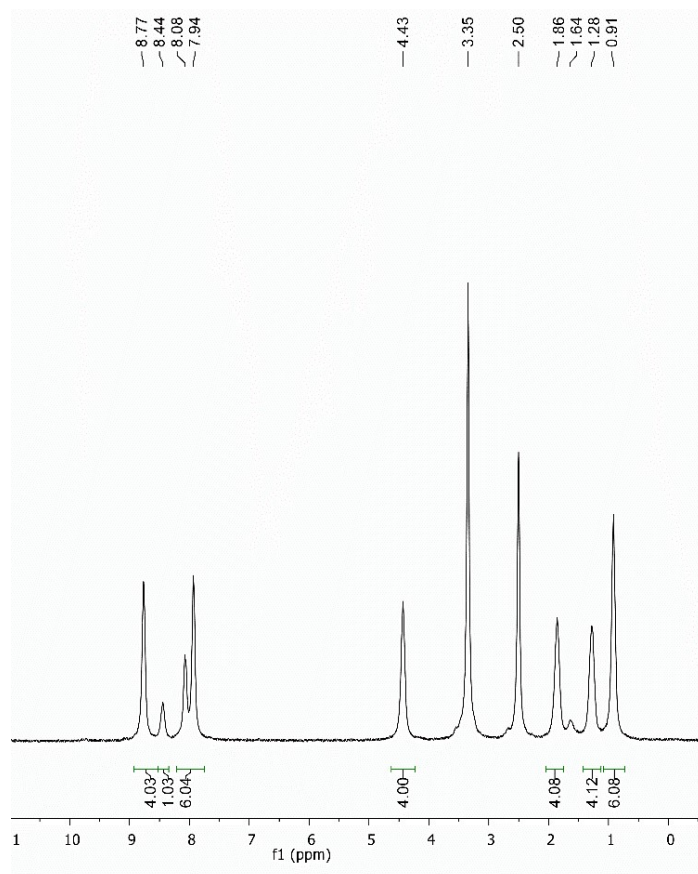


Figure 10.1. ¹H NMR spectrum of **10**

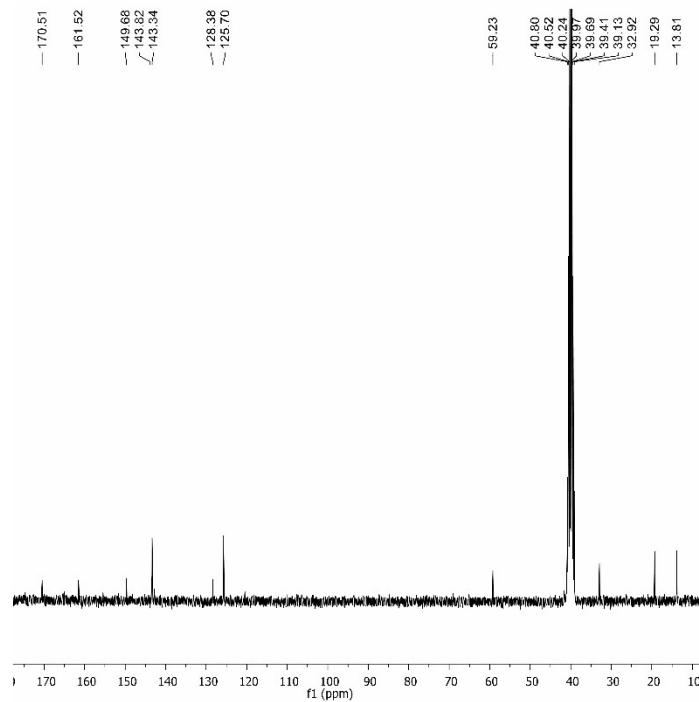


Figure 10.2. ^{13}C NMR spectrum of **10**

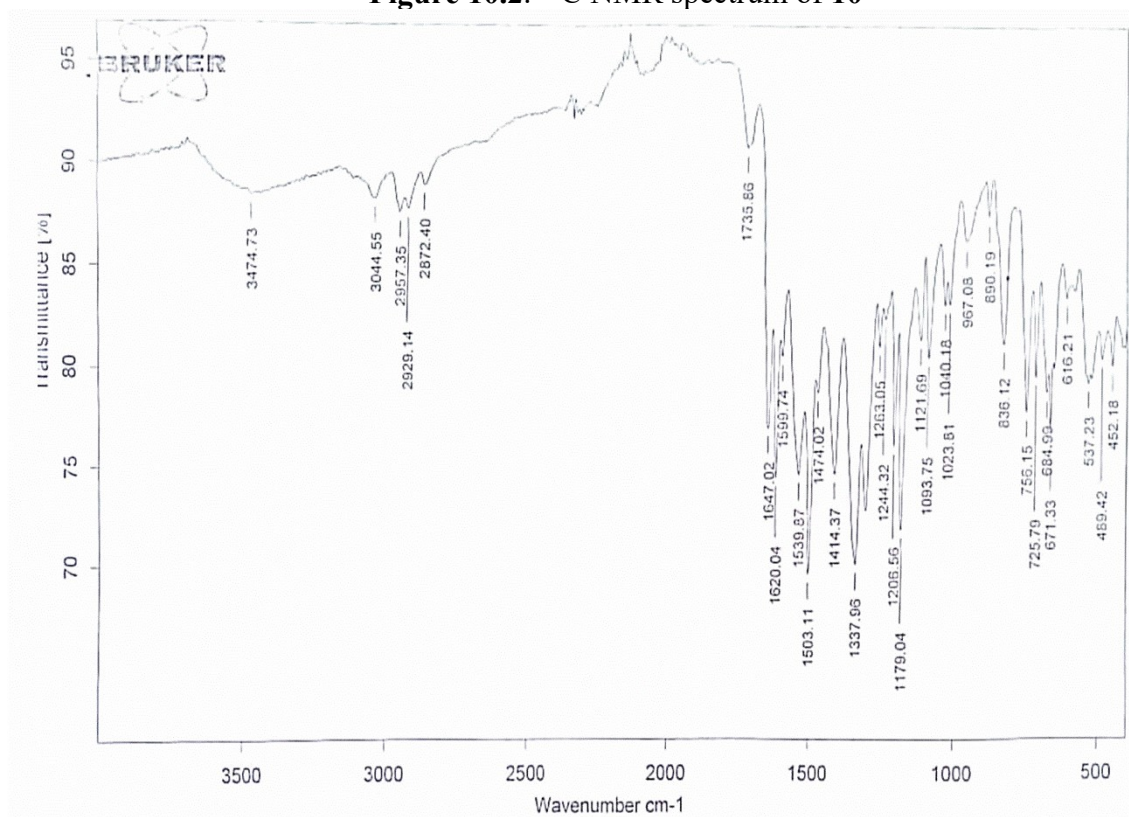


Figure 10.3. Representative FT-IR spectrum of **10**

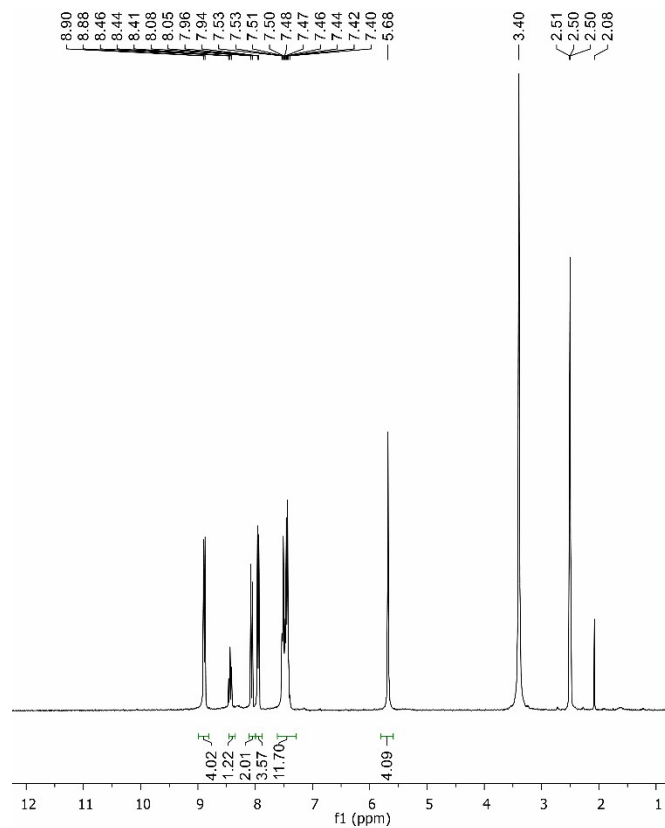


Figure 11.1. ^1H NMR spectrum of **11**

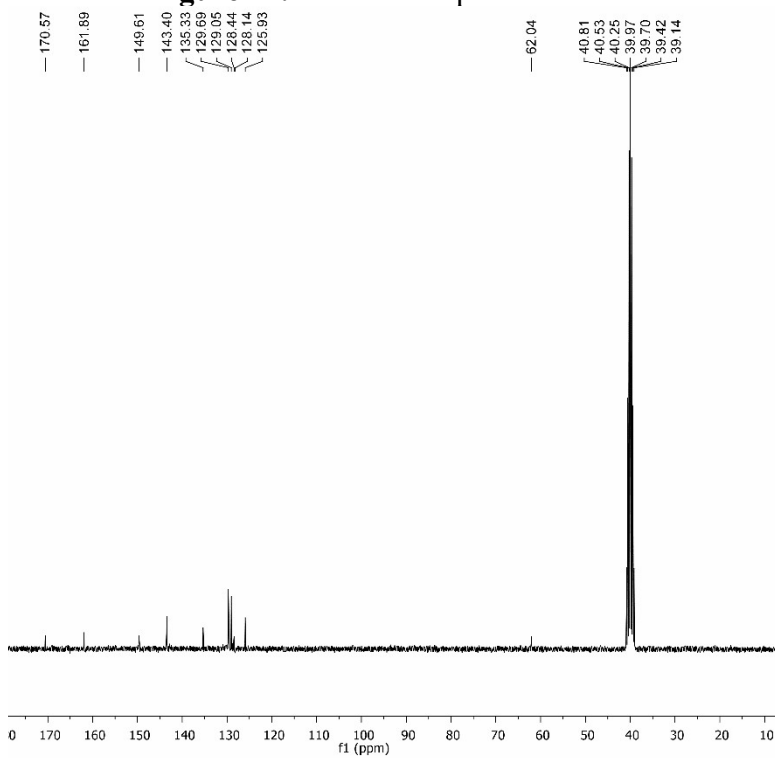


Figure 11.2. ^{13}C NMR spectrum of **11**

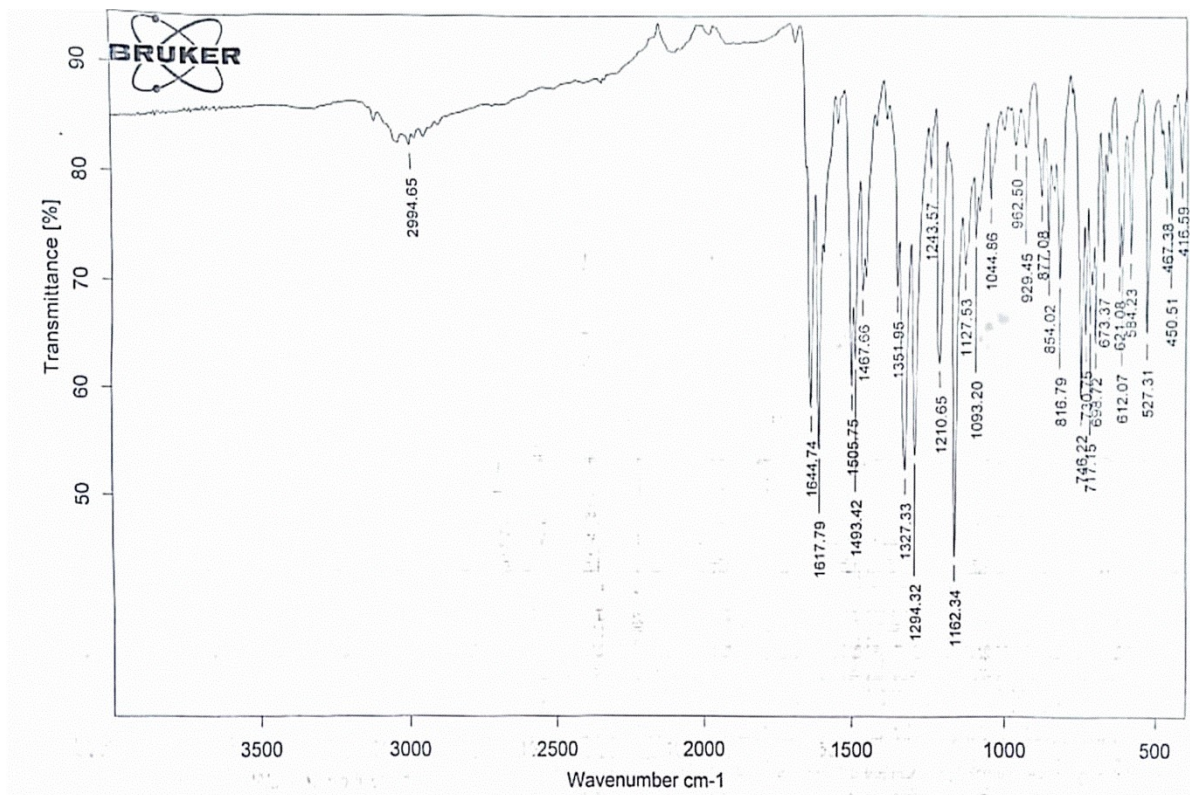


Figure 11.3. Representative FT-IR spectrum of 11

Crystallographic Data: CCDC numbers of **2**, **4** and **11** are 2281737, 2281738, 2281739.

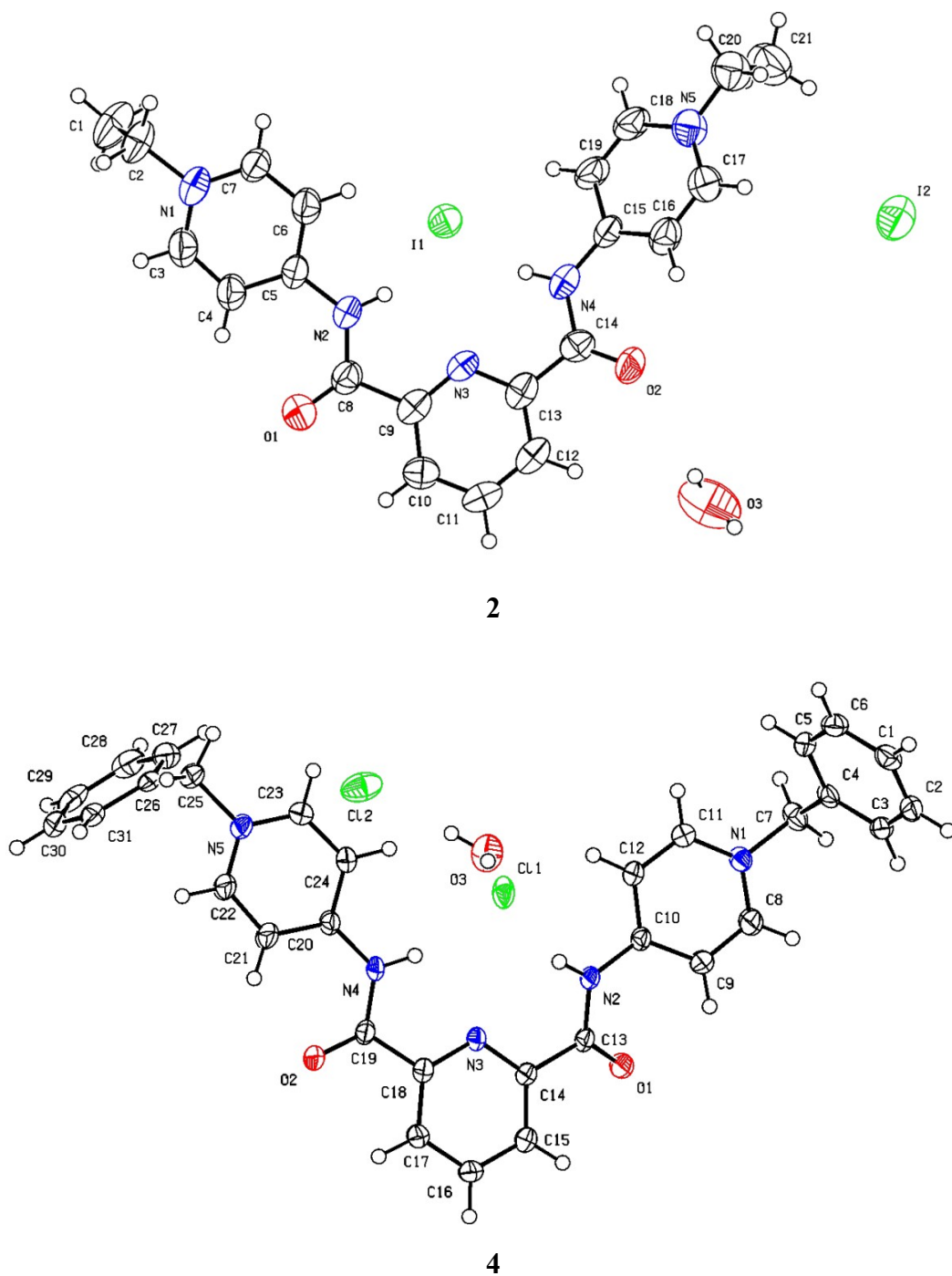
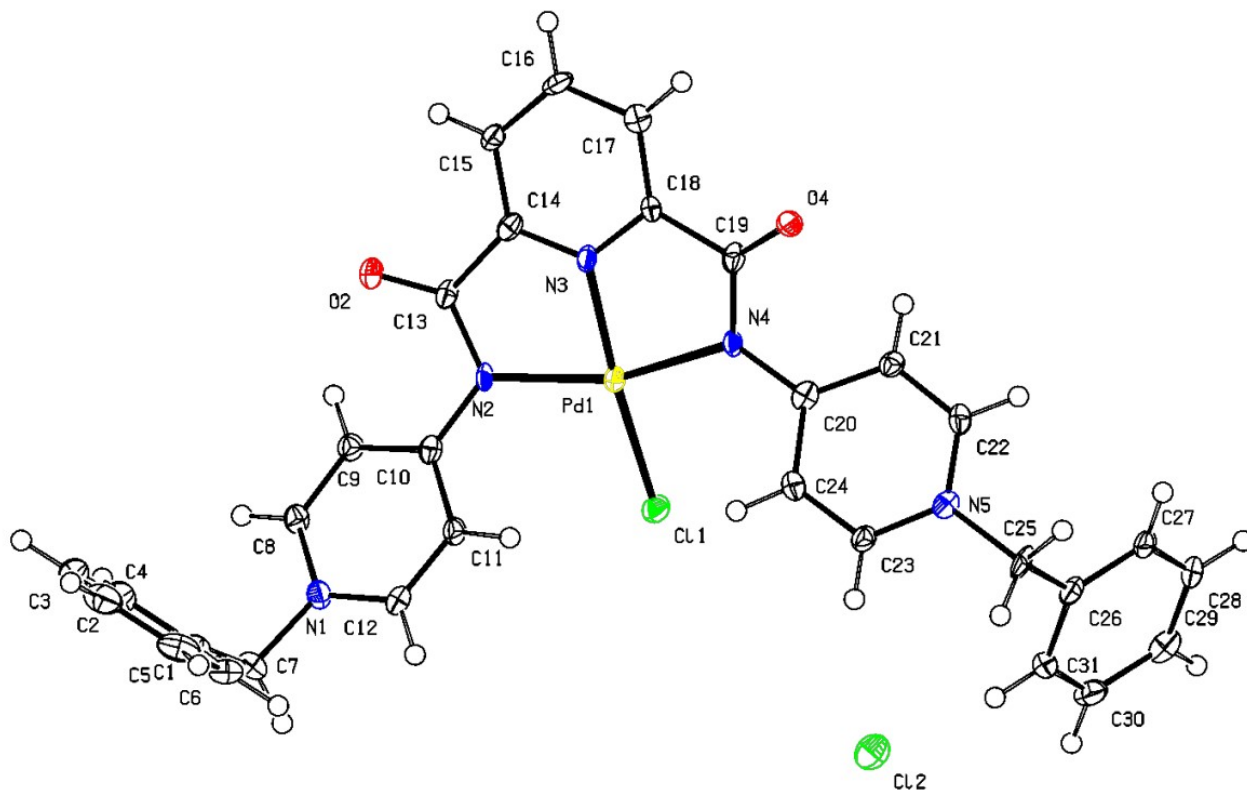


Figure S12. ORTEP diagrams of **2** and **4**



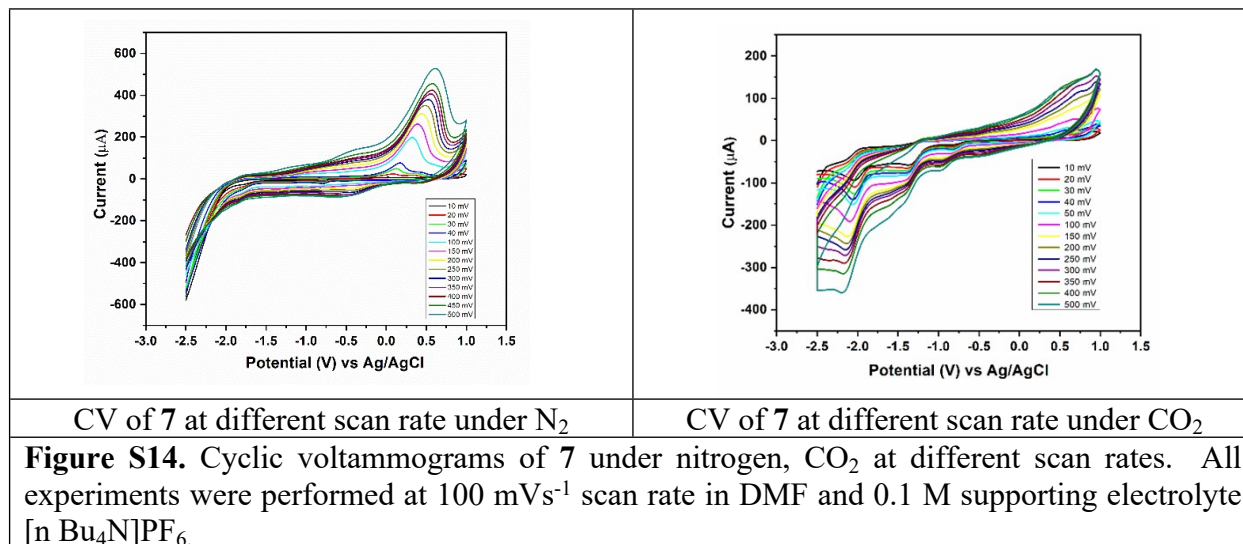
11

Figure S13. ORTEP diagrams of **11**

Single crystals of **2** and **4** suitable for x-ray diffraction analysis, were obtained *via* slow evaporation method. **2** was recrystallized from saturated mixture of water, methanol and acetonitrile. **4** was crystallized out from methanol. ORTEP diagrams of **2** and **4** are given in Figure S12 which evaluates the successful ethylation and benzylation of **1** respectively. The C-N bond distance of N2-C5 and N4-C15 were 1.378(1) Å and 1.385(2) Å respectively in **2** while in **4**, C20-N4 and C10-N2 were 1.382(5) Å and 1.391(6) Å respectively, which is closed to C-N bond length 1.47 Å¹. In **2** the bond lengths of O1-C8 and O2-C14 were 1.227(2) Å and C14 1.202(2) Å respectively while in **4** the bond lengths of C13-O1 and C19-O2 were 1.218(4) Å and 1.214(6) Å respectively, representing carbon oxygen double bond character.

Single crystal of **11** suitable for x-ray diffraction analysis was grown in mixture of acetonitrile, methanol and water *via* slow evaporation method. An ORTEP and packing diagram of **11** is given in Figure S12. It has P2₁/n space group and two molecules packed in unit cell. The C20-N4 and C10-N2 bond lengths extended from 1.382(5) Å to 1.388(8) Å and 1.391(6) Å to 1.394(6) Å in contrast to its respective proligand **4**, due to the shifting of electron density from nitrogen to the palladium. Palladium coordinated with three nitrogen atoms (N2, N3 and N4) of ligand and one chlorine atom (Cl1). The angle between palladium and the three nitrogen atoms (N2-Pd1-N3) and (N3-Pd1-N4) were 80.8(2)° and 80.7(2)° respectively. This distorted square planner geometry of the complex may be due to the rigidity of tridentate ligand.

Electrochemical Activity:



Plots of Peak Current vs. (Scan Rate)^{1/2}

Randles-Sevcik equation describes that the peak current is directly proportional to the square root of the scan rate in an electrochemical redox reaction. A linear plot of the peak current vs the square root of the scan rate demonstrates that the electroactive species in a redox reaction are freely diffusing. Randles-Sevcik plots of the 2 mM complexes (7) under an inert atmosphere and CO_2 are given in Figure S15.

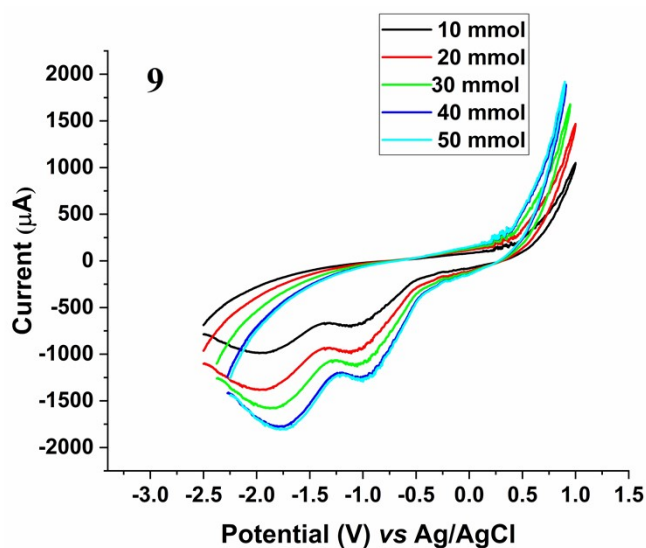
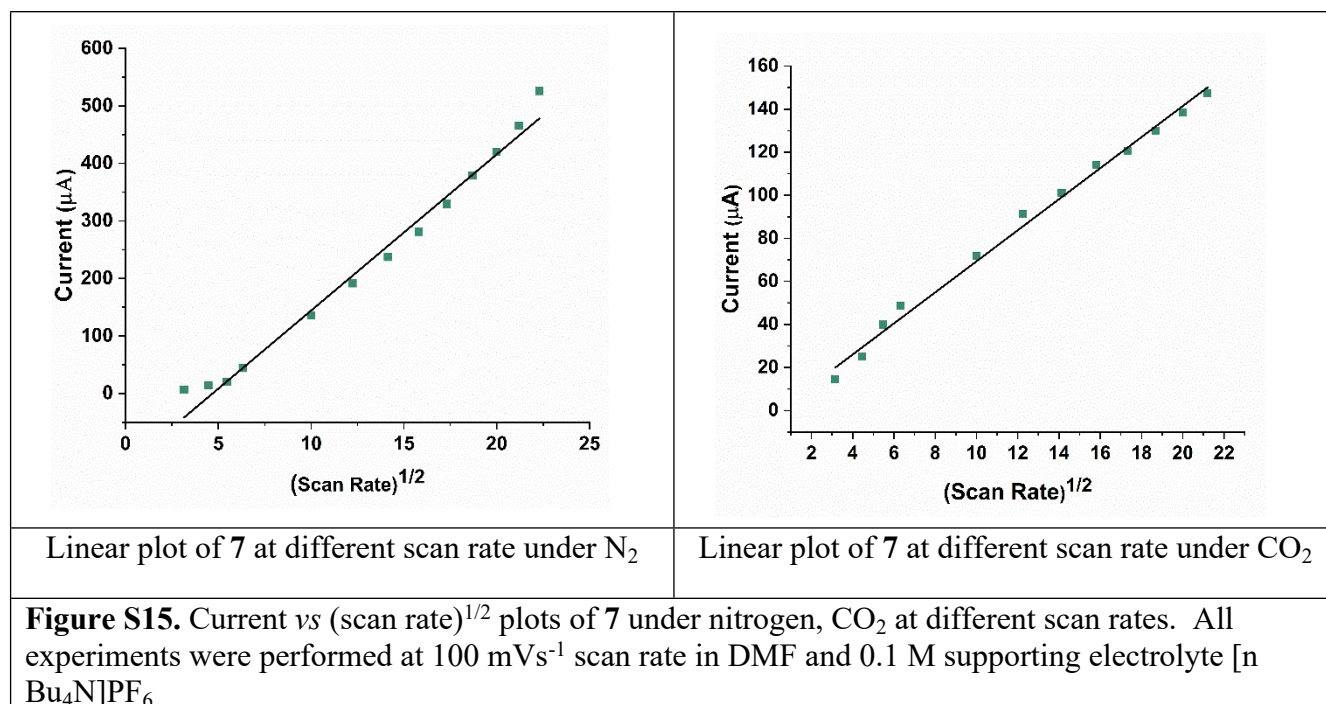


Figure S16. Cyclic voltammograms of **9** under CO₂ + TFA at different concentrations. All experiments were performed at 100 mVs⁻¹ scan rate in DMF and 0.1 M supporting electrolyte ([n Bu₄N]PF₆)

References:

- Allen, F. H.; Kennard, O.; Watson, D. G.; Brammer, L.; Orpen, A. G.; Taylor, R., Tables of bond lengths determined by X-ray and neutron diffraction. Part 1. Bond lengths in organic compounds. *Journal of the Chemical Society, Perkin Transactions 2* **1987**, (12), S1-S19.